

Universal neural network potentials as descriptors: Towards scalable chemical property prediction using quantum and classical computers

Tomoya Shiota,^{1,2,*} Kenji Ishihara,^{2,†} and Wataru Mizukami^{1,2,‡}

¹*Graduate School of Engineering Science, Osaka University,
1-3 Machikaneyama, Toyonaka, Osaka 560-8531, Japan*

²*Center for Quantum Information and Quantum Biology,
Osaka University, 1-2 Machikaneyama, Toyonaka 560-8531, Japan*

(Dated: February 29, 2024)

Accurate prediction of diverse chemical properties is crucial for advancing molecular design and materials discovery. Here we present a versatile approach that uses the intermediate information of a universal neural network potential as a general-purpose descriptor for chemical property prediction. Our method is based on the insight that by training a sophisticated neural network architecture for universal force fields, it learns transferable representations of atomic environments. We show that transfer learning with a graph neural network potential M3GNet achieves accuracy comparable to state-of-the-art methods for predicting the NMR chemical shifts of ¹H, ¹³C, ¹⁵N, ¹⁷O, and ¹⁹F using quantum machine learning as well as a standard classical regression model, despite the compactness of its descriptors. This work provides an efficient way to accurately predict properties, potentially accelerating the discovery of new molecules and materials.

I. INTRODUCTION

As evidenced by the enumeration of 166.4B possible organic molecules containing up to 17 heavy elements, such as C, N, O, S, and halogens (excluding hydrogen), the expansion of the chemical space is astronomical with the increase in types and numbers of elements.[1, 2] This vast landscape has given rise to a multidisciplinary approaches to combining experimental and computational chemistry for the discovery of new chemical substances and materials in a wide range of fields, including material, catalysis, and drug design.[1–6] Although quantum chemistry and first-principles calculations offer accurate descriptions of chemical substances, their high computational demands make an exhaustive exploration of the chemical space impractical.[6–12] However, machine- and deep-learning techniques are overcoming these limitations to enable a more extensive exploration.[4, 6, 10, 13–27]

With machine learning, physics-inspired descriptors that characterize the chemical space have been developed and serve as the cornerstone for building efficient and highly accurate models.[21, 23, 28–40] Smooth overlap of atomic positions (SOAP)[14, 18, 21, 28, 31, 32, 41], Faber–Christensen–Huang–Lilienfeld (FCHL)[29, 30, 33, 34, 38], and similar descriptors offer atom-level descriptions within molecular or material environments based on physical insights and are effective in regressing chemical quantities, such as interatomic potentials (IAP) and nuclear magnetic resonance (NMR) chemical shifts.[11, 14, 15, 21, 23, 24, 28–38, 41–43] Notably, IAPs built using descriptors and Gaussian Process Regression (GPR) [14] have been termed Gaussian approximation potentials (GAP) and have found success in the exploration of

the chemical space of molecules and materials.[14, 21, 37] Both kernel ridge regression (KRR) and GPR have been employed to improve the accuracy of NMR chemical shift prediction [29, 30, 41–44]. However, the dimensionality of the descriptors becomes a barrier to generalization and high accuracy as the molecular or material composition becomes more diverse owing to the addition of different types of elements.[19, 35, 39, 45]

Recently, deep-learning models based on graph neural networks (GNNs) have been proposed to describe chemical spaces using graph representations.[9, 17–20, 24, 25, 45–57] In most GNN-based IAPs, atoms within a molecular or material environment are represented as nodes, and their local connectivity as edges in a graph. The graph is then convolved to embed atom-specific information within each node, and further processed using multilayer perceptrons (MLP) to predict target observables. Numerous high-quality GNN-based IAPs have been developed for screening high-accuracy first-principles calculations and proposing molecular and crystal structures. Universal graph-based IAPs capable of comprehensively handling molecules and materials, such as MEGNet[52], M3GNet[10], Allegro[58], GNoME[59], and MACE[60–62] have emerged and are advancing rapidly.

Similarly, GNN-based models have been developed to predict NMR chemical shifts.[46, 47, 49, 50, 53, 57] For example, Yanfei Guan et al. achieved an accuracy of 0.16 ppm for ¹H and 1.26 ppm for ¹³C by training the SchNet architecture [51] on molecular NMR chemical shifts (CASCADE)[46]. However, the scalability remains an issue due to the increasing optimization costs of GNN and MLP parameters when the size of datasets increase. Han et al. addressed this issue by constraining the nodes in a GNN to heavy elements only, thereby rendering the construction of scalable GNN-based NMR chemical shift models feasible while achieving a state-of-the-art prediction accuracy comparable to that of CASCADE.[53]

Notably, both descriptor-based and GNN methods face

* shiota.tomoya.ss@gmail.com

† ishihara-ke@office.osaka-u.ac.jp

‡ mizukami.wataru.qiqb@osaka-u.ac.jp

challenges. The former faces increased learning costs as the composition becomes more complex, and the latter faces increasing parameter optimization costs with larger training datasets. To address these issues simultaneously, we focused on the potential utility of the outputs from pre-trained GNN-based IAPs as descriptors. We considered these outputs GNN transfer learning (GNN-TF) descriptors and built machine-learning models for predicting chemical properties. Note that there are existing studies attempting to apply pre-trained GNN potentials to other tasks, particularly to generative modeling. [63–66]

The remainder of this paper is organized as follows. Section II details the GNN-TF descriptor and the kernel method, implemented on both classical and quantum computers, for predicting NMR chemical shifts of ^1H , ^{13}C , ^{15}N , ^{17}O , and ^{19}F . Section III presents the performance of our developed machine learning models. Section IV discusses the benefits and applications of the GNN-TF descriptor. Finally, Section V concludes the paper.

II. METHOD: TRANSFER LEARNING USING PRE-TRAINED GRAPH NEURAL NETWORK

In this section, we discuss the transfer learning of a pre-trained GNN-based IAP. This approach integrates the outputs from the GNN layer of the IAP as shown in Fig. 1.

The architecture of a GNN-based IAP can be broadly segmented into a GNN layer and an MLP layer (gray area of Fig. 1). For the IAP, we opted for two backbones: a MEGNet pre-trained on the QM9 dataset[67] and a M3GNet trained on the MPF.2021.2.8 dataset, which encompasses compounds covering all 89 elements from the Materials Project.[10]

The parameters of the GNN layer in the M3GNet IAP have been optimized for the prediction of system energy, forces, and stress tensors. When fed with the coordinates, \mathbf{R}_i s, of a molecule with N atoms, the GNN layer generates a vector, \mathbf{G}_i , which mirrors the environment of the i th atom in the molecule—henceforth referred to as the GNN-TF descriptor.

The GNN layer for both MEGNet and M3GNet outputs GNN-TF descriptors with dimensions of 32 and 64 per atom, respectively. Using GNN-TF descriptors as input, a regression model was constructed to predict NMR chemical shielding constants.

For the regressor, one can choose methodologies, such as GPR, KRR, or feed-forward neural network (NNs), which are contingent on the specific task. In this study, to ensure a maximally fair comparison with other descriptor-based techniques, we adopted KRR.

KRR combines the merits of ridge regression, which offers regularization to mitigate overfitting, with the kernel method, facilitating nonlinear regression. In kernel meth-

ods, the data—in the context of our study, the GNN-TF descriptors—are mapped into a high-dimensional feature space through a non-linear kernel function. The Laplacian kernel, which is known to produce favorable results for chemical properties prediction [13, 29, 68], was employed

$$k(\mathbf{G}_i, \mathbf{G}_j) = \exp(-\gamma \|\mathbf{G}_i - \mathbf{G}_j\|_1), \quad (1)$$

where γ represents the hyperparameter of the kernel. In KRR, the predicted value $\hat{\sigma}_t$ for the target chemical property of the target atom is derived from the GNN-TF descriptor \mathbf{G}_t as follows:

$$\hat{\sigma}_t(\mathbf{G}_t) = \sum_i^N \alpha_i k(\mathbf{G}_i, \mathbf{G}_t) \quad (2)$$

Here, α_i represents the i^{th} element of the regression coefficient vector, $\boldsymbol{\alpha}$, of size N . The regression coefficients are determined by solving a ridge-regularized least-squares problem, which can be reduced to:

$$\boldsymbol{\alpha} = (\mathbf{K} + \lambda \mathbf{I})^{-1} \boldsymbol{\sigma} \quad (3)$$

where \mathbf{I} denotes the identity matrix, $\boldsymbol{\sigma}$ denotes the chemical properties of each N training data samples, and λ denotes the regularization parameter. The matrix \mathbf{K} , is a kernel matrix, with elements given by $k(\mathbf{G}_i, \mathbf{G}_j)$.

All computations related to the KRR were executed using Scikit-learn v.1.2.2,[69] and the hyperparameters of each model were tuned using Optuna v.2.10.[70] The hyperparameters of all models were obtained using only one random 80:20 split of the dataset. We employed five-fold cross-validation for all hyperparameter optimizations. For dataset sizes of up to 50K items, we conducted hyperparameter optimization for 100 iterations, whereas for datasets containing 100K items, we limited the optimization to 50 iterations.

The quantum-kernel method leverages quantum computers to compute kernels, [16, 71, 72] which is achieved by embedding feature vectors generated by classical computers into quantum states. This method calculates the inner product of these quantum states to derive the desired kernels. Embedding feature vectors into quantum states corresponds to mapping them onto a Hilbert space with dimensions raised to the power of two quantum bits (qubits). Using the kernel matrix constructed on a quantum computer, we performed a quantum kernel ridge regression (KRR), commonly referred to as quantum KRR (QKRR).

In this study, we adopted the natural parameterized quantum circuits (NPQC) Kernel, which has been demonstrated to possess performance characteristics similar to the Gaussian kernel, both theoretically and in actual hardware experiments [73–75]. All computations were conducted using Scikit-qulacs [69, 76, 77]. The quantum kernel was constructed in a 10-qubit space. Hyperparameters for the quantum kernel were determined through grid search. The determined parameters

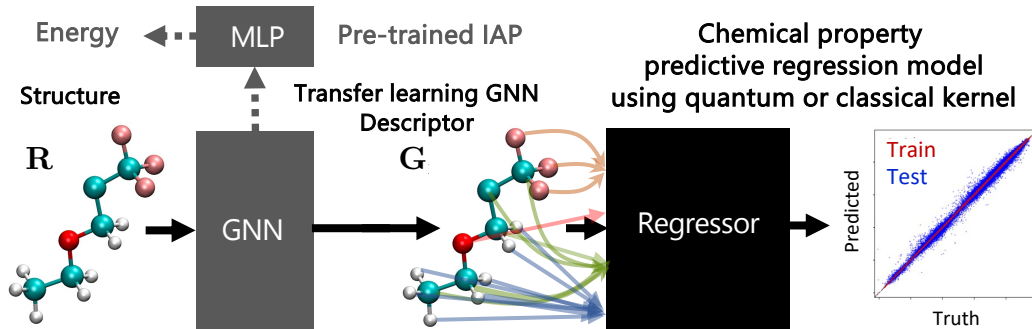


FIG. 1. Schematic diagram of our proposed graph neural network transfer learning for predicting chemical properties. The black arrows depict the flow of our transfer learning process. The gray area is a pre-trained NNP designed for predicting the energy of the system and composed of a GNN and an MLP. The initial step in our learning procedure involves obtaining the pre-trained GNN block output \mathbf{G} using the system’s atomic coordinates \mathbf{R} as input. Subsequently, we construct a regression model to predict the chemical properties *e.g.* NMR shielding constants, using this GNN output \mathbf{G} as a descriptor.

of NPQC kernel were $c = 1.5$ and the repetition times of embedding 40. The regularization hyperparameter in QKRR was determined using 10 iterations of randomized search.

III. RESULTS

In Section III A, because we deal with many elements, we compared the dimensional efficiency of our proposed GNN-TF descriptor to well-established physics-inspired descriptors. Note that the GNN-TF descriptor can better handle complex chemical systems by exploiting the GNN-based IAP architecture.

In Section III B, we focused on the accuracy of the GNN-TF descriptor in predicting NMR chemical shifts, which are key to understanding molecular details (*e.g.*, interatomic distances and bond angles). This scenario provides an ideal test for determining how well the GNN-TF descriptor works in our study.

Our analysis began by comparing quantum kernel learning, in which the kernels are tested using a quantum computer emulator with traditional kernel learning methods. We then checked the accuracy of the GNN-TF descriptors across the different pretrained GNN models.

Finally, we juxtaposed our GNN-TF descriptor using well-established physics-inspired descriptors. This comparison demonstrates the superiority of the proposed descriptor in terms of efficiency and accuracy. Furthermore, it highlights its potential for accurately predicting chemical properties, which is crucial for advancing research in the molecular and material sciences.

A. Dimensional Efficiency

At the atomic level, descriptors are tools designed to encode information about atoms within molecules or

crystalline materials into vectors. Popular descriptors, such as SOAP and FCHL18, excel at intricately capturing the environment within an atom’s cutoff radius.

Although these descriptors have achieved significant success in various accuracy benchmarks, they also present challenges due to their large dimensions. Various strategies have been developed to address these challenges,[34, 79–81] including refining the descriptor itself, using principal component analysis for dimensionality reduction, and exploring NNs to encode them. In particular, Christensen et al. applied Behler’s method of the atom-centered symmetry function [82] for NN potential to discretize FCHL18[33] to derive a compact and accurate FCHL19.[34]

In Table I, we present the scaling of the SOAP, FCHL19, and M3GNet GNN-TF descriptors in response to an increase in the number of elemental species considered. Additionally, for the QM9, QMugs,[83] and MPF.2021.8 datasets,[10] the descriptor dimensions corresponding to 5, 10, and 89 elemental species comprising each dataset are summarized, respectively.

Remarkably, with an increase in the number of element types, both SOAP and FCHL19 exhibited quadratic scaling. As a snapshot, when representing five elements in

TABLE I. Scaling of descriptor dimensions with respect to number of elements.

	SOAP ^a	FCHL19 ^a	M3GNet GNN-TF
Scaling with respect to N_{elem}	$O(N_{\text{elem}}^2)$	$O(N_{\text{elem}}^2)$	$O(1)$
$N_{\text{elem}} = 5(\text{QM9})$	5740	740	64
$N_{\text{elem}} = 10(\text{QMugs})$	22680	2440	64
$N_{\text{elem}} = 89(\text{MPF.2021.2.8})$	1737120	162336	64

^a SOAP and FCHL were generated by Dscribe 0.4.0[28] and QML 0.4.0.12[78], respectively. The default hyperparameters were selected as in QM9NMR paper.

the QM9 dataset, the SOAP and FCHL19 methods have dimensions of 5,740 and 740, respectively. This dimensional disparity increases with the number of elemental types. Hence, to represent the 89 elements, the dimensions increased to 1,737,120 and 162,336, respectively. This is tens-of-thousands times larger than the concise 64 dimensions of the M3GNet GNN-TF descriptor.

Owing to its consistent dimensionality, irrespective of the increase in elements, the GNN-TF descriptor is overwhelmingly compact.

B. Prediction Accuracy: NMR Chemical Shifts

The NMR chemical shifts, δ , were predicted using the chemical shielding constant of the reference substance, σ_{ref} , as the baseline. The NMR chemical shift was calculated using the following equation:

$$\delta = \sigma_{\text{ref}} - \sigma. \quad (4)$$

The reference substances selected for the various nuclei in this study are widely recognized and commonly adopted in the literature.[29, 84–87] Specifically, tetramethylsilane was selected for both ^1H and ^{13}C , nitromethane (MeNO_2) for ^{15}N , water- ^{17}O (H_2^{17}O) for ^{17}O , and trichlorofluoromethane (CFC_13) for ^{19}F . We determined the chemical shielding constants for these well-established reference substances as follows: 31.7608 ppm for ^1H , 187.0521 ppm for ^{13}C , -147.8164 ppm for ^{15}N , 325.8642 ppm for ^{17}O , and 171.2621 ppm for ^{19}F . These constants were evaluated by calculations at the mPW1PW91/6-311+G(2d,p) level using density functional theory (DFT) and gauge-including atomic orbital (GIAO) methods. Structure optimization was conducted at the B3LYP/6-31G(2df,p) level in alignment with the methodologies employed for the QM9 NMR dataset. All calculations were performed using the Gaussian 16 software suite.[88]

In our study, we utilized the QM9NMR dataset, which contains approximately 134K small organic molecules containing C, N, O, and F (excluding H), with each molecule having no more than nine atoms.[29, 67] This dataset provides the detailed NMR chemical shielding constants for these molecules. To analyze how the model accuracy changes with training data size, we adopted an approach similar to that used in the original publication of the QM9NMR dataset.[29] Specifically, for ^{13}C , of a total of 831K data points, we randomly withheld 50K data points to build our test set. Subsequently, from the remaining ^{13}C NMR chemical shifts, we randomly selected subsets containing 100, 200, 500, 1K, 2K, 5K, 10K, 50K, 100K, and 200K data points to create various training sets. For the other isotopes (i.e., ^1H , ^{15}N , ^{17}O , and ^{19}F), the test sets were similarly established by withholding 50K, 30K, 50K, and 1K data points, respectively. The training size for ^{19}F was set to 2K, whereas the other isotopes were trained on datasets of 100K data points. In addition to the QM9 NMR dataset, we sought

to validate the performance of our model on external datasets. Hence, we employed the two sets of molecules provided in another study;[29] one consisting of 40 drug molecules from the GDB17 universe and another containing 12 drugs with 17 or more heavy atoms.

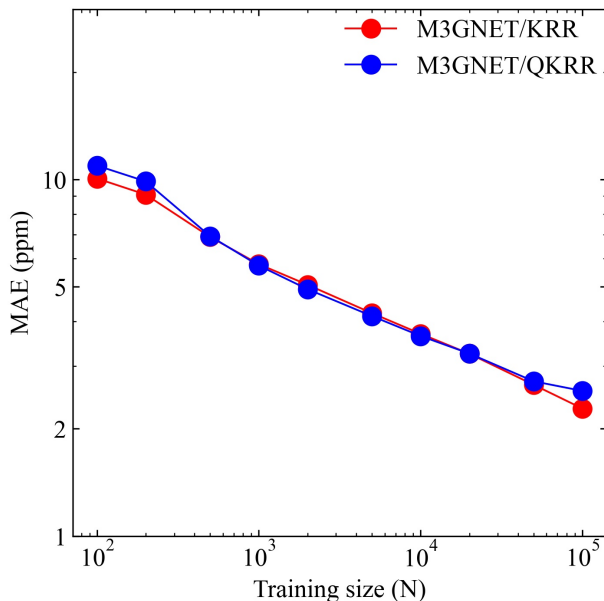


FIG. 2. Log-log plot of the training size (N) and MAE for the ^{13}C NMR chemical shielding constant prediction model. The red and blue colors represent the results of the KRR and QKRR models using GNN-TF descriptors from the pre-trained M3GNet model, respectively.

Figure 2 shows the relationship between the mean absolute error (MAE) for ^{13}C NMR shielding constant predictions and the training data size. Both QKRR and KRR demonstrated consistent improvements in predictive accuracy with an increase in training size. Notably, the quantum kernel exhibited a performance comparable to that of the Laplacian kernel.

For a training size of 100K, the MAE for the ^{13}C predictions was 2.28 ppm. In a comparative study by Gupta et al., the KRR models using the Coulomb matrix (CM),[89] SOAP, and FCHL descriptors reported MAEs of approximately 4, 2.1, and 1.88 ppm, respectively, for the same training size.[29]

Compared with the CM descriptor, our GNN-TF descriptor showed significantly better predictive capabilities, achieving an MAE that was nearly half that of the CM descriptor. Although our method did not exceed the accuracy levels of SOAP and FCHL, the performance of the GNN-TF descriptor was competitive, highlighting its potential as a robust descriptor.

Next, we compared the performance of the GNN-TF descriptors derived from different IAP architectures.

Recently, independent of our work, a predictive model for ^{13}C NMR chemical shielding was proposed using a

pretrained IAP known as SchNet, which is a pioneering GNN used as a descriptor.[90] This model was trained on 400 data points of ^{13}C NMR chemical shielding constants of the molecules in QM9 dataset,[67] with the SchNet GNN-TF descriptor as an input to a feed-forward NN for regression. The predictive accuracy of the SchNet/NN was 12.8 ppm.

In pursuit of a fair comparison with their model, we applied Kernel Ridge Regression (KRR) using pre-trained M3GNet and MEGNet GNN-TF descriptors, setting our training data size to 400 data points of ^{13}C NMR chemical shielding constants. The results of this comparative study are summarized in Table II.

The highest predictive accuracy was achieved by the M3GNet/KRR model, with an root mean-squared error of 10.0 ppm. This value surpassed the 20.4 ppm achieved by the MEGNet/KRR model and the 12.8 ppm achieved by the SchNet/NN model. This clearly underscores the superior performance of the M3GNet GNN descriptor over the other GNN-TF descriptors.

These results suggest that the architecture of the GNN-based IAP influences the performance of the GNN-TF descriptor. A more detailed discussion of the nuances of these architectural differences is presented in Section IV A.

The accuracy of KRR models incorporating the GNN-TF descriptor for NMR chemical shifts was evaluated for molecules containing five elements that were not present in the training dataset. Table III lists the statistical performance metrics for predicting NMR chemical shifts. Across all elements, the MAE for the test set remained below 5 ppm. The MAE for ^1H and ^{19}F were notably low at 0.18 ppm and 2.65 ppm, respectively, indicating a high degree of prediction accuracy for these nuclei in the unseen molecules. The MAE for ^{17}O , although higher at 4.95 ppm, still reflects a reasonable predictive capability, given the complexity of the oxygen chemical shifts. The standard deviation (STD) and interquartile range (IQR) values in the table represent the distribution of chemical shifts within the training data, rather than the accuracy of the model itself. Thus, the higher STD and IQR values for ^{17}O do not indicate a lack of model precision but rather the natural variability inherent in the ^{17}O chemical shifts within the training data. The MAE/STD ratio can still offer insights into model performance relative to data variability. For example, the relatively low ratio of ^{17}O (2.21%) suggests that the model predictions are consistent with the diversity of the training data. Similarly,

TABLE II. The architecture dependence of the predictive performance

GNN-TF descriptor/Regressor	RMSE (ppm)
SchNet/NN ^a	12.8
MEGNet/KRR	20.4
M3GNet/KRR	10.0

^a The value is taken from [90]

TABLE III. Predictive performance and data variability of NMR shielding constants for 5 elements

	^1H	^{13}C	^{15}N	^{17}O	^{19}F
MAE (ppm)	0.18	2.28	3.42	4.95	2.65
STD (ppm)	1.98	51.96	119.58	224.40	34.07
IQR (ppm)	2.34	59.93	211.19	354.25	36.77
MAE/STD (%)	8.93	4.38	2.86	2.21	7.78

TABLE IV. The MAE values for the prediction of the 50k QM9NMR hold out set, 40 drug molecules from GDB17 Universe and the other containing 12 drugs with 17 or more heavy atoms

	FCHL ^a	M3GNet GNN-TF
50K QM9	1.88	2.28
40 drugs	3.7	3.47
12 drugs	4.2	4.23

^a FCHL results are taken from [29].

the higher ratios for ^1H and ^{19}F indicate that the accuracy of the model is commendable, particularly when considering the broad range of chemical shifts represented in the training dataset.

Subsequently, these models were employed to predict the NMR chemical shifts of molecules containing five elements that were not included in the training data. The results are shown in Fig. 3. The MAE for each nucleus were found to be 0.08 ppm for ^1H , 1.03 ppm for ^{13}C , 6.45 ppm for ^{15}N , 2.86 ppm for ^{17}O , and 6.73 ppm for ^{19}F . The remarkably low MAE for ^1H and ^{13}C underscores the high accuracy of our model for these nuclei, with predictions that closely mirror the calculated values. The model performed well for the more challenging ^{15}N and ^{17}O nuclei, where the chemical shifts can be significantly affected by subtle changes in the molecular structure and environment, as indicated by the MAE values. The ^{19}F nucleus, while having a higher MAE, showed excellent agreement with the DFT/GIAO calculations, suggesting that the model predictions were robust, even for nuclei with typically higher chemical shift ranges. These results demonstrate the strong predictive power and potential of the model as a reliable tool for accurately predicting NMR chemical shifts across a variety of nuclei, even in molecules beyond the scope of the training data.

We then expanded our assessment to evaluate the predictive ability of our model for molecules larger than those in the QM9 NMR dataset. As such, we incorporate the test sets provided in another study,[29] which comprised 40 drug molecules from the GDB17 universe and another set containing 12 drugs with 17 or more heavy atoms.

Table IV presents the benchmark results for these test sets using our M3GNet GNN-TF descriptor. For comparison, we used the FCHL descriptor from Gupta’s study.[29] To ensure a fair comparison, we employed our M3GNet GNN-TF descriptor model trained on a size of

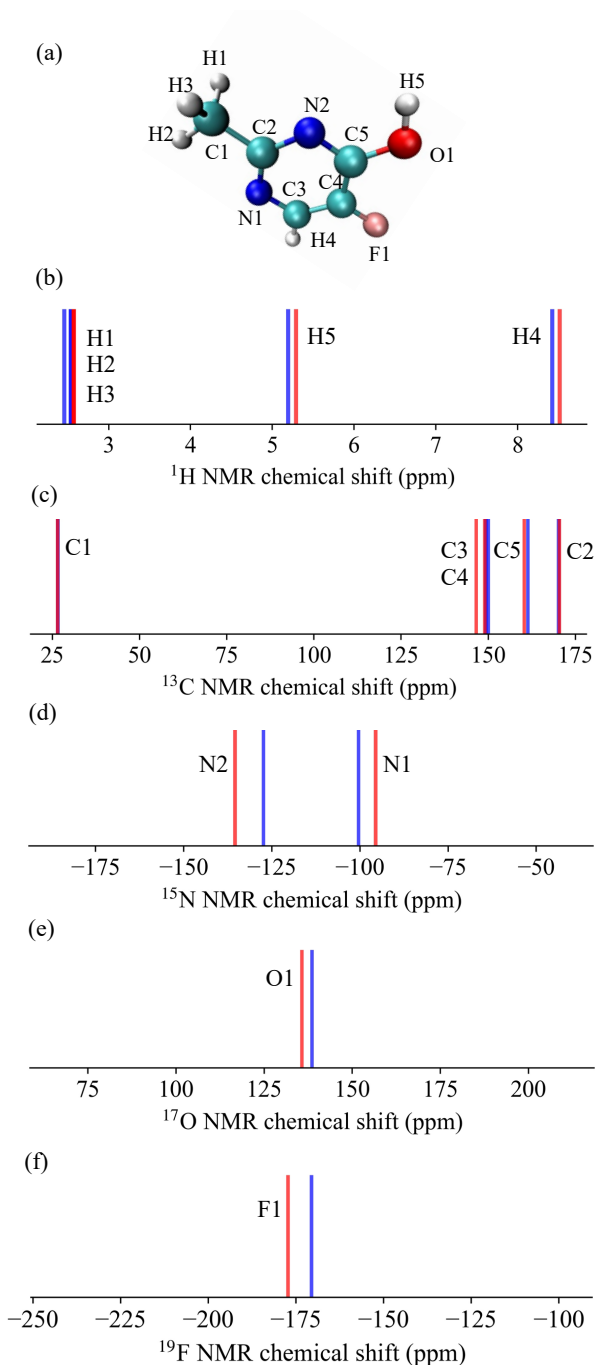


FIG. 3. Predicted NMR chemical shifts for (a) a single molecule, randomly selected from the QM9NMR dataset and not included in the training data, for (b) ^1H , (c) ^{13}C , (d) ^{15}N , (e) ^{17}O , and (f) ^{19}F . These predictions (represented by red lines) are compared with the calculated values at the DFT/GIAO level, which are considered as the correct values (depicted by blue lines).

100K ^{13}C . For both models, an increased molecular size in the dataset correlated with deterioration of the MAE value. Notably, although our M3GNet GNN-TF descriptor did not match the 1.88 ppm value achieved by the FCHL descriptor for the QM9 50K test set, our model exhibited an MAE value that was approximately 0.3 ppm lower for the 40 GDB17 dataset test. The results were nearly identical for the set of 12 drugs with 17 or more heavy atoms, highlighting that the GNN-TF descriptor was less affected by increasing molecular size.

For a detailed comparison, Fig. 4 illustrates the molecule-specific MAE values for both drug test sets. The molecular structures are provided in Appendix B, and more intricate details are available in another study.[29] Our M3GNet GNN-TF descriptor-based prediction model ensured that the highest MAE values for individual molecules across both test sets remained below 10 ppm. Intriguingly, the desflurane molecule, which posed the greatest challenge, showed MAE values of 53.3 ppm and 9.35 ppm for the FCHL and M3GNet GNN-TF descriptor models, respectively. This suggests an approximately 80% reduction in the MAE with our descriptor, which is likely attributable to differences in the encompassed descriptor domain.

The cutoff radius for the FCHL descriptor was determined through a grid search,[29] which settled at 4.0 Å. In this scenario, the two fluorine atoms in the terminal trifluoromethyl group (CF_3) of the desflurane molecule, which lie beyond 4 Å from the CF_2H carbon, were neglected. In contrast, our M3GNet descriptor had a 6 Å cutoff radius during the initial graph configuration and a 5 Å cutoff for three-body interactions during graph convolution, capturing the entire CF_3 group. This suggests that the descriptor adequately accounts for the influence of the terminal trifluoromethyl group. Additionally, the intrinsic ability of GNN-TF descriptors to account for environments beyond their cutoff radius, owing to graph convolution, may have contributed to the substantial improvement in MAE.

In summary, the proposed M3GNet GNN-TF descriptor demonstrates the capability of predicting ^{13}C NMR chemical shifts for molecules outside the training dataset with an accuracy comparable to that of the state-of-the-art FCHL descriptor.

IV. DISCUSSION

A. Influence of Architectural Choices on GNN-TF Descriptor Performance

In our exploration of different architectures for generating GNN-TF descriptors, we observed several patterns. SchNet, which operates on GNN-based local descriptors to evaluate systems as summations of atomic energies, accounts only for pairwise interactions. This limited inclusion could potentially constrain expressions, leading to inadequate representational power.

The subpar performance of MEGNet during transfer learning may be attributed to its architectural design as it integrates atomic (local) descriptors into molecular (global) descriptors through concatenation. This means that the final piece of information passed to the MLP is not extracted directly from the end of the model, which might not be the optimal representation for targeted atomic-wise property prediction; however, it is expected to be suitable for molecule-wise property predictions.

B. Significance of Dataset Size and Diversity

The M3GNet training regimen incorporates data from 187,687 ionic steps spanning 62,783 compounds, including 187,687 energies, 16,875,138 force components, and 1,689,183 stress components. This diverse dataset covers 89 elements from the periodic table. The model is not limited to learning only the energies associated with these elements but extends to atomic-level forces. Moreover, M3GNet training includes not only stable structures but also the processes of structure optimization. The ingestion of vast amounts of data from crystalline systems may have endowed the M3GNet with enhanced expression, potentially making it adept at interpolating molecular systems.

C. Potential for Transfer Learning on Quantum Computer

There is a potential for leveraging quantum computation approaches.[91] Specifically, our 10 qubit QKRR, facilitated by a simulator, demonstrated a performance comparable to that of state-of-the-art KRR. This is underpinned by the theoretical equivalence of the NPQC with the RBF.

The quantum kernel method stands out because of its capability to compute with fewer measurement iterations than other quantum computation methodologies, such as quantum neural networks.[92] In particular, our proposed M3GNet GNN-TF descriptor can be feasibly realized with a minimum of six qubits, enabling evaluations with a quantum bit count that is more efficient than traditional descriptors, such as SOAP. However, embedding for higher-dimensional SOAP appears to be a challenge, possibly due to noise.

From a futuristic perspective, there is excitement about the possibility of developing kernels that traditional computers cannot express, as well as accelerating the inversion calculations of kernel matrices using quantum algorithms. The constant scaling property of our proposed method concerning element number dimensions may significantly contribute to real-time material exploration powered by quantum-classical hybrid algorithms in the near future.

V. CONCLUSION

The dynamics of machine learning and its extensive applications across various domains are driving cutting-edge research. Our endeavor to integrate transfer learning with pretrained IAP GNNs for NMR chemical shift prediction offers a paradigm shift in efficiency and scalability. The GNN-TF descriptor presents an unparalleled advantage in terms of scalability due to its consistent dimensionality, irrespective of the number of elements.

Comparative evaluations with other renowned descriptors, such as SOAP, suggest that the GNN-TF descriptor can match, if not surpass, the performance of its contemporaries while maintaining a more compact representation. This is especially important when factoring large datasets, where dimensionality can exponentially burgeon.

Architectural choice plays a pivotal role in the performance of GNN-TF descriptors. Moreover, the diversity and vastness of the training dataset, which encompasses myriad elemental types and structural configurations, augment the robustness and versatility of the GNN.

Our proposed model has immense potential for creating a unified framework capable of predicting various atomic and molecular properties simultaneously, presenting profound implications for accelerated material and molecular research. This potential union of multiple predictions can usher in an era of comprehensive understanding and quicker innovations, possibly revolutionizing fields, such as catalysis, drug discovery, and material design.

The union of transfer learning with pretrained GNNs not only augments prediction accuracy but also drastically reduces learning costs, presenting a cost-effective and efficient alternative to more computationally intensive methods. As we move toward an era in which data-driven insights and models govern the pace of innovation, our research offers a promising pathway for future endeavors in the domain of chemical property predictions with both classical and quantum computers.

Note added - As we were finalizing this manuscript, we became aware of recent articles [90, 93, 94] that also utilize intermediate information from graph neural network potentials. In Section IIIB, we added a direct comparison between our results and theirs. Elijošius et al. applied the pre-trained MACE descriptor to generative modeling of molecules [94].

ACKNOWLEDGMENTS

We thank Nobuki Inoue and Tuan Minh Do for fruitful discussions. This project was supported by funding from the MEXT Quantum Leap Flagship Program (MEXTQLEAP) through Grant No. JPMXS0120319794, and the JST COI-NEXT Program through Grant No. JP-MJPF2014. The completion of this research was partially

facilitated by the JSPS Grants-in-Aid for Scientific Research (KAKENHI), specifically Grant Nos. JP23H03819 and JP21K18933. We thank the Supercomputer Center, the Institute for Solid State Physics, the University of Tokyo for the use of the facilities. This work was also

achieved through the use of SQUID at the Cybermedia Center, Osaka University.

-
- [1] J.-L. Reymond, R. van Deursen, L. C. Blum, and L. Ruddigkeit, *Chemical space as a source for new drugs*, *MedChemComm* **1**, 30 (2010).
- [2] L. Ruddigkeit, R. van Deursen, L. C. Blum, and J.-L. Reymond, *Enumeration of 166 billion organic small molecules in the chemical universe database GDB-17*, *Journal of Chemical Information and Modeling* **52**, 2864 (2012).
- [3] R. Gómez-Bombarelli, J. Aguilera-Iparraguirre, T. D. Hirzel, D. Duvenaud, D. Maclaurin, M. A. Blood-Forsythe, H. S. Chae, M. Einzinger, D.-G. Ha, T. Wu, G. Markopoulos, S. Jeon, H. Kang, H. Miyazaki, M. Numata, S. Kim, W. Huang, S. I. Hong, M. Baldo, R. P. Adams, and A. Aspuru-Guzik, *Design of efficient molecular organic light-emitting diodes by a high-throughput virtual screening and experimental approach*, *Nature Materials* **15**, 1120 (2016).
- [4] S. Curtarolo, G. L. W. Hart, M. B. Nardelli, N. Mingo, S. Sanvito, and O. Levy, *The high-throughput highway to computational materials design*, *Nature Materials* **12**, 191 (2013).
- [5] W. Nie, Q. Wan, J. Sun, M. Chen, M. Gao, and S. Chen, *Ultra-high-throughput mapping of the chemical space of asymmetric catalysis enables accelerated reaction discovery*, *Nature Communications* **14**, 10.1038/s41467-023-42446-5 (2023).
- [6] A. R. Oganov, C. J. Pickard, Q. Zhu, and R. J. Needs, *Structure prediction drives materials discovery*, *Nature Reviews Materials* **4**, 331 (2019).
- [7] G. K. Pierens, *1h and 13c nmr scaling factors for the calculation of chemical shifts in commonly used solvents using density functional theory*, *Journal of computational chemistry* **35**, 1388 (2014).
- [8] J. D. Hartman, R. A. Kudla, G. M. Day, L. J. Mueller, and G. J. O. Beran, *Benchmark fragment-based 1h, 13c, 15n and 17o chemical shift predictions in molecular crystals*, *Physical Chemistry Chemical Physics* **18**, 21686 (2016).
- [9] J. B. K. Büning and S. Grimme, *Computation of CCSD(t)-quality NMR chemical shifts via machine learning from DFT*, *Journal of Chemical Theory and Computation* **19**, 3601 (2023).
- [10] C. Chen and S. P. Ong, *A universal graph deep learning interatomic potential for the periodic table*, *Nature Computational Science* **2**, 718 (2022).
- [11] M. W. Lodewyk, M. R. Siebert, and D. J. Tantillo, *Computational prediction of 1h and 13c chemical shifts: A useful tool for natural product, mechanistic, and synthetic organic chemistry*, *Chemical Reviews* **112**, 1839 (2011).
- [12] G. Lauro, P. Das, R. Riccio, D. S. Reddy, and G. Bifulco, *Dft/nmr approach for the configuration assignment of groups of stereoisomers by the combination and comparison of experimental and predicted sets of data*, *The Journal of Organic Chemistry* **85**, 3297–3306 (2020).
- [13] K. Hansen, F. Biegler, R. Ramakrishnan, W. Pronobis, O. A. Von Lilienfeld, K.-R. Muller, and A. Tkatchenko, *Machine learning predictions of molecular properties: Accurate many-body potentials and nonlocality in chemical space*, *The journal of physical chemistry letters* **6**, 2326 (2015).
- [14] V. L. Deringer, A. P. Bartók, N. Bernstein, D. M. Wilkins, M. Ceriotti, and G. Csányi, *Gaussian process regression for materials and molecules*, *Chemical Reviews* **121**, 10073 (2021).
- [15] F. A. Faber, L. Hutchison, B. Huang, J. Gilmer, S. S. Schoenholz, G. E. Dahl, O. Vinyals, S. Kearnes, P. F. Riley, and O. A. von Lilienfeld, *Prediction errors of molecular machine learning models lower than hybrid dft error*, *Journal of Chemical Theory and Computation* **13**, 5255 (2017).
- [16] M. Sajjan, J. Li, R. Selvarajan, S. H. Sureshbabu, S. S. Kale, R. Gupta, V. Singh, and S. Kais, *Quantum machine learning for chemistry and physics*, *Chemical Society Reviews* **51**, 6475 (2022).
- [17] J. A. Keith, V. Vassilev-Galindo, B. Cheng, S. Chmiela, M. Gastegger, K.-R. Müller, and A. Tkatchenko, *Combining machine learning and computational chemistry for predictive insights into chemical systems*, *Chemical Reviews* **121**, 9816 (2021).
- [18] K. Wan, J. He, and X. Shi, *Construction of high accuracy machine learning interatomic potential for surface/interface of nanomaterials—a review*, *Advanced Materials* 10.1002/adma.202305758 (2023).
- [19] Z. Wu, B. Ramsundar, E. N. Feinberg, J. Gomes, C. Geniesse, A. S. Pappu, K. Leswing, and V. Pande, *MoleculeNet: a benchmark for molecular machine learning*, *Chemical Science* **9**, 513 (2018).
- [20] P. Reiser, M. Neubert, A. Eberhard, L. Torresi, C. Zhou, C. Shao, H. Metni, C. van Hoesel, H. Schopmans, T. Sommer, and P. Friederich, *Graph neural networks for materials science and chemistry*, *Communications Materials* **3**, 10.1038/s43246-022-00315-6 (2022).
- [21] A. P. Bartók, S. De, C. Poelking, N. Bernstein, J. R. Kermode, G. Csányi, and M. Ceriotti, *Machine learning unifies the modeling of materials and molecules*, *Science Advances* **3**, 10.1126/sciadv.1701816 (2017).
- [22] E. Kocer, T. W. Ko, and J. Behler, *Neural network potentials: A concise overview of methods*, *Annual Review of Physical Chemistry* **73**, 163–186 (2022).
- [23] M. F. Langer, A. Goeßmann, and M. Rupp, *Representations of molecules and materials for interpolation of quantum-mechanical simulations via machine learning*, *npj Computational Materials* **8**, 41 (2022).
- [24] Z. Liu, L. Lin, Q. Jia, Z. Cheng, Y. Jiang, Y. Guo, and J. Ma, *Transferable multilevel attention neural network for accurate prediction of quantum chemistry properties via multitask learning*, *Journal of Chemical Information*

- and Modeling **61**, 1066–1082 (2021).
- [25] A. Merchant, S. Batzner, S. S. Schoenholz, M. Aykol, G. Cheon, and E. D. Cubuk, Scaling deep learning for materials discovery, *Nature* **624**, 80–85 (2023).
- [26] P. Gao, J. Zhang, Q. Peng, J. Zhang, and V.-A. Glezakou, General protocol for the accurate prediction of molecular $^{13}\text{C}/^1\text{H}$ nmr chemical shifts via machine learning augmented dft, *Journal of Chemical Information and Modeling* **60**, 3746 (2020).
- [27] S. J. Y. Macalino, V. Gosu, S. Hong, and S. Choi, Role of computer-aided drug design in modern drug discovery, *Archives of Pharmacal Research* **38**, 1686 (2015).
- [28] L. Himanen, M. O. Jäger, E. V. Morooka, F. Federici Canova, Y. S. Ranawat, D. Z. Gao, P. Rinke, and A. S. Foster, Dscribe: Library of descriptors for machine learning in materials science, *Computer Physics Communications* **247**, 106949 (2020).
- [29] A. Gupta, S. Chakraborty, and R. Ramakrishnan, Revving up ^{13}C NMR shielding predictions across chemical space: benchmarks for atoms-in-molecules kernel machine learning with new data for 134 kilo molecules, *Machine Learning: Science and Technology* **2**, 035010 (2021).
- [30] W. Gerrard, L. A. Bratholm, M. J. Packer, A. J. Mulholland, D. R. Glowacki, and C. P. Butts, IMPRESSION – prediction of NMR parameters for 3-dimensional chemical structures using machine learning with near quantum chemical accuracy, *Chemical Science* **11**, 508 (2020).
- [31] M. J. Willatt, F. Musil, and M. Ceriotti, Atom-density representations for machine learning, *The Journal of Chemical Physics* **150**, 10.1063/1.5090481 (2019).
- [32] A. P. Bartók, R. Kondor, and G. Csányi, On representing chemical environments, *Physical Review B* **87**, 10.1103/physrevb.87.184115 (2013).
- [33] F. A. Faber, A. S. Christensen, B. Huang, and O. A. von Lilienfeld, Alchemical and structural distribution based representation for universal quantum machine learning, *The Journal of Chemical Physics* **148**, 10.1063/1.5020710 (2018).
- [34] A. S. Christensen, L. A. Bratholm, F. A. Faber, and O. A. von Lilienfeld, FCHL revisited: Faster and more accurate quantum machine learning, *The Journal of Chemical Physics* **152**, 10.1063/1.5126701 (2020).
- [35] A. Kabylda, V. Vassilev-Galindo, S. Chmiela, I. Poltavsky, and A. Tkatchenko, Efficient interatomic descriptors for accurate machine learning force fields of extended molecules, *Nature Communications* **14**, 10.1038/s41467-023-39214-w (2023).
- [36] F. Musil, A. Grisafi, A. P. Bartók, C. Ortner, G. Csányi, and M. Ceriotti, Physics-inspired structural representations for molecules and materials, *Chemical Reviews* **121**, 9759 (2021).
- [37] A. P. Bartók, M. C. Payne, R. Kondor, and G. Csányi, Gaussian approximation potentials: The accuracy of quantum mechanics, without the electrons, *Physical Review Letters* **104**, 10.1103/physrevlett.104.136403 (2010).
- [38] B. Parsaeifard, D. Sankar De, A. S. Christensen, F. A. Faber, E. Kocer, S. De, J. Behler, O. Anatole von Lilienfeld, and S. Goedecker, An assessment of the structural resolution of various fingerprints commonly used in machine learning, *Machine Learning: Science and Technology* **2**, 015018 (2021).
- [39] D. Khan, S. Heinen, and O. A. von Lilienfeld, Kernel based quantum machine learning at record rate: Many-body distribution functionals as compact representations, *The Journal of Chemical Physics* **159**, 10.1063/5.0152215 (2023).
- [40] M. Rupp, R. Ramakrishnan, and O. A. von Lilienfeld, Machine learning for quantum mechanical properties of atoms in molecules, *The Journal of Physical Chemistry Letters* **6**, 3309 (2015).
- [41] M. Cordova, E. A. Engel, A. Stefaniuk, F. Paruzzo, A. Hofstetter, M. Ceriotti, and L. Emsley, A machine learning model of chemical shifts for chemically and structurally diverse molecular solids, *The Journal of Physical Chemistry C* **126**, 16710 (2022).
- [42] K. J. Kohlhoff, P. Robustelli, A. Cavalli, X. Salvatella, and M. Vendruscolo, Fast and accurate predictions of protein NMR chemical shifts from interatomic distances, *Journal of the American Chemical Society* **131**, 13894 (2009).
- [43] M. Tsitsvero, J. Pirillo, Y. Hijikata, and T. Komatsuzaki, Nmr spectrum prediction for dynamic molecules by machine learning: A case study of trefoil knot molecule, *The Journal of Chemical Physics* **158**, 10.1063/5.0147398 (2023).
- [44] F. M. Paruzzo, A. Hofstetter, F. Musil, S. De, M. Ceriotti, and L. Emsley, Chemical shifts in molecular solids by machine learning, *Nature Communications* **9**, 10.1038/s41467-018-06972-x (2018).
- [45] V. Fung, J. Zhang, E. Juarez, and B. G. Sumpter, Benchmarking graph neural networks for materials chemistry, *npj Computational Materials* **7**, 10.1038/s41524-021-00554-0 (2021).
- [46] Y. Guan, S. V. S. Sowndarya, L. C. Gallegos, P. C. S. John, and R. S. Paton, Real-time prediction of ^1H and ^{13}C chemical shifts with DFT accuracy using a 3d graph neural network, *Chemical Science* **12**, 12012 (2021).
- [47] S. Liu, J. Li, K. C. Bennett, B. Ganoe, T. Stauch, M. Head-Gordon, A. Hexemer, D. Ushizima, and T. Head-Gordon, Multiresolution 3d-DenseNet for chemical shift prediction in NMR crystallography, *The Journal of Physical Chemistry Letters* **10**, 4558 (2019).
- [48] H. Han and S. Choi, Transfer learning from simulation to experimental data: NMR chemical shift predictions, *The Journal of Physical Chemistry Letters* **12**, 3662 (2021).
- [49] Y. Kwon, D. Lee, Y.-S. Choi, M. Kang, and S. Kang, Neural message passing for NMR chemical shift prediction, *Journal of Chemical Information and Modeling* **60**, 2024 (2020).
- [50] E. Jonas and S. Kuhn, Rapid prediction of NMR spectral properties with quantified uncertainty, *Journal of Cheminformatics* **11**, 10.1186/s13321-019-0374-3 (2019).
- [51] K. T. Schütt, P.-J. Kindermans, H. E. Sauceda, S. Chmiela, A. Tkatchenko, and K.-R. Müller, Schnet: A continuous-filter convolutional neural network for modeling quantum interactions (2017), arXiv:1706.08566 [stat.ML].
- [52] C. Chen, W. Ye, Y. Zuo, C. Zheng, and S. P. Ong, Graph networks as a universal machine learning framework for molecules and crystals, *Chemistry of Materials* **31**, 3564 (2019).
- [53] J. Han, H. Kang, S. Kang, Y. Kwon, D. Lee, and Y.-S. Choi, Scalable graph neural network for NMR chemical shift prediction, *Physical Chemistry Chemical Physics* **24**, 26870 (2022).
- [54] K. Xu, W. Hu, J. Leskovec, and S. Jegelka, How power-

- ful are graph neural networks? (2019), arXiv:1810.00826 [cs.LG].
- [55] H. Stärk, D. Beaini, G. Corso, P. Tossou, C. Dallago, S. Günnemann, and P. Lió, 3D infomax improves GNNs for molecular property prediction, in *Proceedings of the 39th International Conference on Machine Learning*, Proceedings of Machine Learning Research, Vol. 162, edited by K. Chaudhuri, S. Jegelka, L. Song, C. Szepesvari, G. Niu, and S. Sabato (PMLR, 2022) pp. 20479–20502.
- [56] D. Jiang, Z. Wu, C.-Y. Hsieh, G. Chen, B. Liao, Z. Wang, C. Shen, D. Cao, J. Wu, and T. Hou, Could graph neural networks learn better molecular representation for drug discovery? a comparison study of descriptor-based and graph-based models, *Journal of Cheminformatics* **13**, 10.1186/s13321-020-00479-8 (2021).
- [57] S. Kang, Y. Kwon, D. Lee, and Y.-S. Choi, Predictive modeling of nmr chemical shifts without using atomic-level annotations, *Journal of Chemical Information and Modeling* **60**, 3765–3769 (2020).
- [58] A. Musaelian, S. Batzner, A. Johansson, L. Sun, C. J. Owen, M. Kornbluth, and B. Kozinsky, Learning local equivariant representations for large-scale atomistic dynamics, *Nature Communications* **14**, 579 (2023).
- [59] A. Merchant, S. Batzner, S. S. Schoenholz, M. Aykol, G. Cheon, and E. D. Cubuk, Scaling deep learning for materials discovery, *Nature* 10.1038/s41586-023-06735-9 (2023).
- [60] I. Batatia, D. P. Kovacs, G. N. C. Simm, C. Ortner, and G. Csanyi, MACE: Higher order equivariant message passing neural networks for fast and accurate force fields, in *Advances in Neural Information Processing Systems*, edited by A. H. Oh, A. Agarwal, D. Belgrave, and K. Cho (2022).
- [61] D. P. Kovács, J. H. Moore, N. J. Browning, I. Batatia, J. T. Horton, V. Kapil, I.-B. Magdău, D. J. Cole, and G. Csányi, Mace-off23: Transferable machine learning force fields for organic molecules, arXiv preprint arXiv:2312.15211 (2023).
- [62] I. Batatia, P. Benner, Y. Chiang, A. M. Elena, D. P. Kovács, J. Riebesell, X. R. Advincula, M. Asta, W. J. Baldwin, N. Bernstein, A. Bhowmik, S. M. Blau, V. Cărare, J. P. Darby, S. De, F. D. Pia, V. L. Deringer, R. Elijošius, Z. El-Machachi, E. Fako, A. C. Ferrari, A. Genreith-Schriever, J. George, R. E. A. Goodall, C. P. Grey, S. Han, W. Handley, H. H. Heenen, K. Hermansson, C. Holm, J. Jaafar, S. Hofmann, K. S. Jakob, H. Jung, V. Kapil, A. D. Kaplan, N. Karimitari, N. Kroupa, J. Kullgren, M. C. Kuner, D. Kuryla, G. Liepuoniute, J. T. Margraf, I.-B. Magdău, A. Michaelides, J. H. Moore, A. A. Naik, S. P. Niblett, S. W. Norwood, N. O’Neill, C. Ortner, K. A. Persson, K. Reuter, A. S. Rosen, L. L. Schaaf, C. Schran, E. Sivonxay, T. K. Stenczel, V. Svahn, C. Sutton, C. van der Oord, E. Varga-Umbrich, T. Vegge, M. Vondrák, Y. Wang, W. C. Witt, F. Zills, and G. Csányi, A foundation model for atomistic materials chemistry (2023), arXiv:2401.00096 [physics.chem-ph].
- [63] T. Xie, X. Fu, O.-E. Ganea, R. Barzilay, and T. Jaakkola, Crystal diffusion variational autoencoder for periodic material generation, arXiv preprint arXiv:2110.06197 (2021).
- [64] L. Wu, C. Gong, X. Liu, M. Ye, and Q. Liu, Diffusion-based molecule generation with informative prior bridges, *Advances in Neural Information Processing Systems* **35**, 36533 (2022).
- [65] S. Zaidi, M. Schaarschmidt, J. Martens, H. Kim, Y. W. Teh, A. Sanchez-Gonzalez, P. Battaglia, R. Pascanu, and J. Godwin, Pre-training via denoising for molecular property prediction, arXiv preprint arXiv:2206.00133 (2022).
- [66] S. Jia, A. R. Parthasarathy, R. Feng, G. Cong, C. Zhang, and V. Fung, Derivative-based pre-training of graph neural networks for materials property predictions, *Digital Discovery* (2024).
- [67] R. Ramakrishnan, P. O. Dral, M. Rupp, and O. A. von Lilienfeld, Quantum chemistry structures and properties of 134 kilo molecules, *Scientific Data* **1**, 10.1038/sdata.2014.22 (2014).
- [68] P. O. Dral, O. A. von Lilienfeld, and W. Thiel, Machine learning of parameters for accurate semiempirical quantum chemical calculations, *Journal of chemical theory and computation* **11**, 2120 (2015).
- [69] F. Pedregosa, G. Varoquaux, A. Gramfort, V. Michel, B. Thirion, O. Grisel, M. Blondel, P. Prettenhofer, R. Weiss, V. Dubourg, J. Vanderplas, A. Passos, D. Cournapeau, M. Brucher, M. Perrot, and E. Duchesnay, Scikit-learn: Machine learning in Python, *Journal of Machine Learning Research* **12**, 2825 (2011).
- [70] T. Akiba, S. Sano, T. Yanase, T. Ohta, and M. Koyama, Optuna: A next-generation hyperparameter optimization framework (2019), arXiv:1907.10902 [cs.LG].
- [71] M. Schuld and N. Killoran, Quantum machine learning in feature hilbert spaces, *Physical Review Letters* **122**, 10.1103/physrevlett.122.040504 (2019).
- [72] T. Kusumoto, K. Mitarai, K. Fujii, M. Kitagawa, and M. Negoro, Experimental quantum kernel trick with nuclear spins in a solid, *npj Quantum Information* **7**, 10.1038/s41534-021-00423-0 (2021).
- [73] T. Haug, C. N. Self, and M. S. Kim, Quantum machine learning of large datasets using randomized measurements, *Machine Learning: Science and Technology* **4**, 015005 (2023).
- [74] T. Haug and M. S. Kim, Natural parametrized quantum circuit, *Physical Review A* **106**, 10.1103/physreva.106.052611 (2022).
- [75] M. Benedetti, E. Lloyd, S. Sack, and M. Fiorentini, Parameterized quantum circuits as machine learning models, *Quantum Science and Technology* **4**, 043001 (2019).
- [76] <https://github.com/Qulacs-0saka/scikit-qulacs>.
- [77] Y. Suzuki, Y. Kawase, Y. Masumura, Y. Hiraga, M. Nakadai, J. Chen, K. M. Nakanishi, K. Mitarai, R. Imai, S. Tamiya, T. Yamamoto, T. Yan, T. Kawakubo, Y. O. Nakagawa, Y. Ibe, Y. Zhang, H. Yamashita, H. Yoshimura, A. Hayashi, and K. Fujii, Qulacs: a fast and versatile quantum circuit simulator for research purpose, *Quantum* **5**, 559 (2021).
- [78] A. S. Christensen, L. A. Bratholm, F. A. Faber, B. Huang, A. Tkatchenko, K. R. Müller, and O. A. von Lilienfeld, Qml: A python toolkit for quantum machine learning, <https://github.com/qmlcode/qml> (2017).
- [79] N. Lopanitsyna, G. Fraux, M. A. Springer, S. De, and M. Ceriotti, Modeling high-entropy transition metal alloys with alchemical compression, *Physical Review Materials* **7**, 045802 (2023).
- [80] M. J. Willatt, F. Musil, and M. Ceriotti, Feature optimization for atomistic machine learning yields a data-driven construction of the periodic table of the elements, *Physical Chemistry Chemical Physics* **20**, 29661 (2018).

- [81] S. Li, Y. Liu, D. Chen, Y. Jiang, Z. Nie, and F. Pan, Encoding the atomic structure for machine learning in materials science, *Wiley Interdisciplinary Reviews: Computational Molecular Science* **12**, e1558 (2022).
- [82] J. Behler, Atom-centered symmetry functions for constructing high-dimensional neural network potentials, *The Journal of Chemical Physics* **134**, 074106 (2011).
- [83] C. Isert, K. Atz, J. Jiménez-Luna, and G. Schneider, Qmugs, quantum mechanical properties of drug-like molecules, *Scientific Data* **9**, 273 (2022).
- [84] D. Xin, C. A. Sader, U. Fischer, K. Wagner, P.-J. Jones, M. Xing, K. R. Fandrick, and N. C. Gonnella, Systematic investigation of dft-giao 15n nmr chemical shift prediction using b3lyp/cc-pvdz: application to studies of regioisomers, tautomers, protonation states and n-oxides, *Organic & Biomolecular Chemistry* **15**, 928–936 (2017).
- [85] C. Puzzarini, G. Cazzoli, M. E. Harding, J. Vázquez, and J. Gauss, A new experimental absolute nuclear magnetic shielding scale for oxygen based on the rotational hyperfine structure of h2o17, *The Journal of Chemical Physics* **131**, 10.1063/1.3274062 (2009).
- [86] R. E. Wasylishen and D. L. Bryce, A revised experimental absolute magnetic shielding scale for oxygen, *The Journal of Chemical Physics* **117**, 10061–10066 (2002).
- [87] C. P. Rosenau, B. J. Jelier, A. D. Gossert, and A. Togni, Exposing the origins of irreproducibility in fluorine nmr spectroscopy, *Angewandte Chemie International Edition* **57**, 9528 (2018).
- [88] M. J. Frisch, G. W. Trucks, H. B. Schlegel, G. E. Scuseria, M. A. Robb, J. R. Cheeseman, G. Scalmani, V. Barone, G. A. Petersson, H. Nakatsuji, X. Li, M. Caricato, A. V. Marenich, J. Bloino, B. G. Janesko, R. Gomperts, B. Mennucci, H. P. Hratchian, J. V. Ortiz, A. F. Izmaylov, J. L. Sonnenberg, D. Williams-Young, F. Ding, F. Lipparini, F. Egidi, J. Goings, B. Peng, A. Petrone, T. Henderson, D. Ranasinghe, V. G. Zakrzewski, J. Gao, N. Rega, G. Zheng, W. Liang, M. Hada, M. Ehara, K. Toyota, R. Fukuda, J. Hasegawa, M. Ishida, T. Nakajima, Y. Honda, O. Kitao, H. Nakai, T. Vreven, K. Throssell, J. A. Montgomery, Jr., J. E. Peralta, F. Ogliaro, M. J. Bearpark, J. J. Heyd, E. N. Brothers, K. N. Kudin, V. N. Staroverov, T. A. Keith, R. Kobayashi, J. Normand, K. Raghavachari, A. P. Rendell, J. C. Burant, S. S. Iyengar, J. Tomasi, M. Cossi, J. M. Millam, M. Klene, C. Adamo, R. Cammi, J. W. Ochterski, R. L. Martin, K. Morokuma, O. Farkas, J. B. Foresman, and D. J. Fox, *Gaussian~16 Revision C.01* (2016), gaussian Inc. Wallingford CT.
- [89] M. Rupp, A. Tkatchenko, K.-R. Müller, and O. A. von Lilienfeld, Fast and accurate modeling of molecular atomization energies with machine learning, *Physical Review Letters* **108**, 10.1103/physrevlett.108.058301 (2012).
- [90] A. M. E. Samman, S. D. Castro, B. Morton, and S. D. Baerdemacker, Transfer learning graph representations of molecules for pka, 13c-nmr, and solubility 10.26434/chemrxiv-2023-hfcm5 (2023).
- [91] M. Cerezo, A. Arrasmith, R. Babbush, S. C. Benjamin, S. Endo, K. Fujii, J. R. McClean, K. Mitarai, X. Yuan, L. Cincio, and P. J. Coles, Variational quantum algorithms, *Nature Reviews Physics* **3**, 625 (2021).
- [92] K. Mitarai, M. Negoro, M. Kitagawa, and K. Fujii, Quantum circuit learning, *Physical Review A* **98**, 10.1103/physreva.98.032309 (2018).
- [93] A. El-Samman, I. Husain, M. Huynh, S. De Castro, B. Morton, G. Acke, and S. De Baerdemacker, Global interpretability and geometry of graph convolutional neural networks for chemistry in terms of chemical moieties 10.26434/chemrxiv-2023-zhlmr (2023).
- [94] R. Elijošius, F. Zills, I. Batatia, S. W. Norwood, D. P. Kovács, C. Holm, and G. Csányi, Zero shot molecular generation via similarity kernels, arXiv preprint arXiv:2402.08708 (2024).

Appendix A: Distribution of Datasets for Each NMR Chemical Shift Prediction Model

The distributions of the training and test sets sampled from the QM9NMR dataset are shown in Fig. 4. Figure 4.(b) shows that above 5K, the distribution is in good agreement with the overall distribution of the ^{13}C NMR shielding constants. For the other elemental species, the distributions of the training and test sets were in good agreement with the overall distribution.

Appendix B: Validation of Learning Accuracy of NMR Chemical Shift Prediction

Figure 5 illustrates the accuracy of the KRR models trained using the M3GNet GNN-TF descriptor for five elemental species. The MAE values for the NMR shielding constant, for train/test, are as follows: for ^1H , 0.0344/0.1767; ^{13}C , 0.1420/2.2798 ppm; ^{15}N , 0.3910/3.4157 ppm; ^{17}O 0.8881/4.9509 ppm; and ^{19}F 0.0864/2.6518 ppm.

The structures of two sets of drug molecules [29] used for validating the constructed model beyond the QM9NMR dataset are depicted in Figs. 6 and 7, respectively. The predicted ^{13}C NMR shielding constants for each drug molecule using the M3GNet GNN-TF/KRR model are shown in Fig. 8. These predictions are accompanied by the values predicted by the FCHL/KRR model.[29]

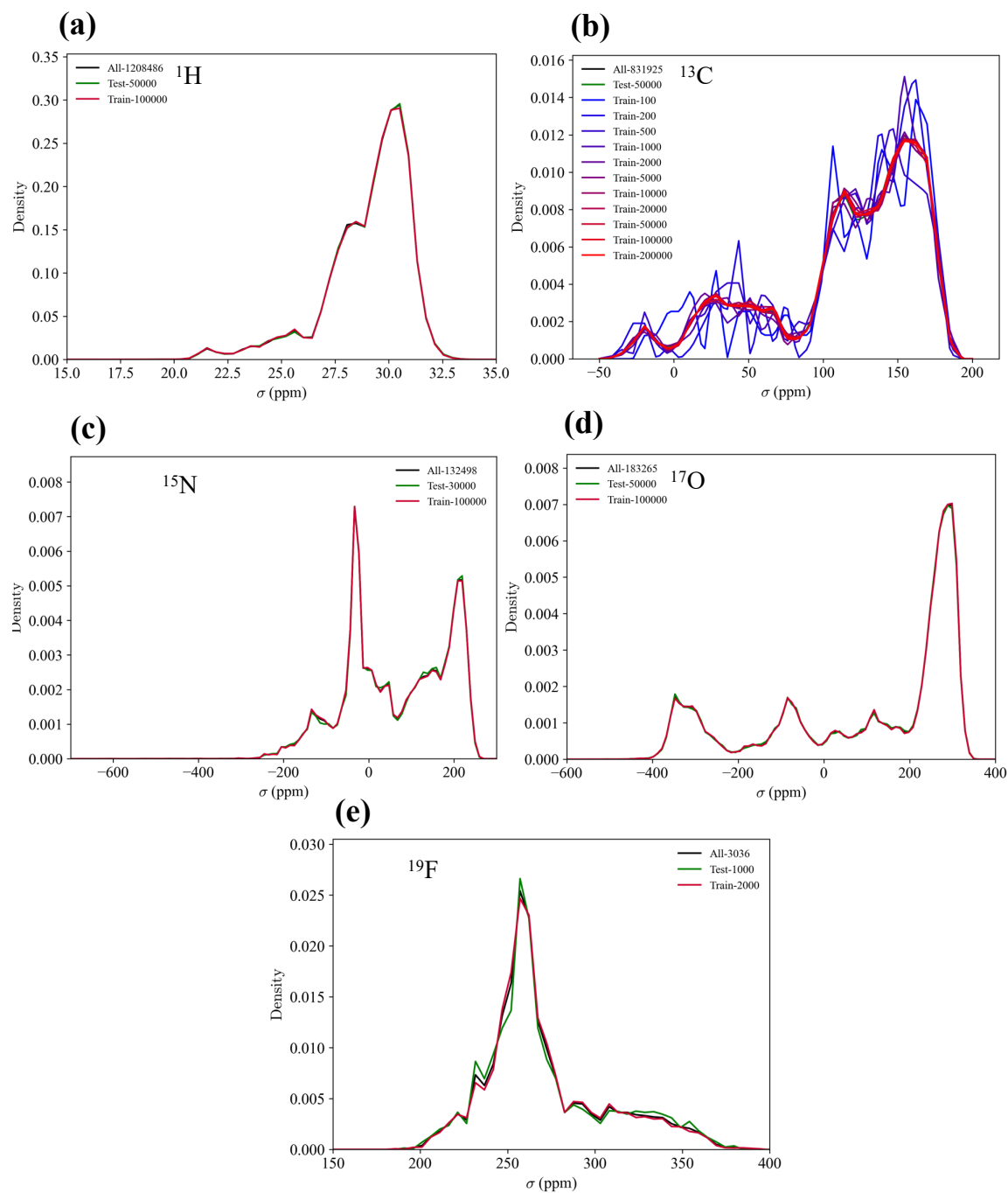


FIG. 4. Distributions of the NMR shielding constants of the training subsets and test set sampled from the of the QM9NMR dataset for the five elemental species: (a) ^1H , (b) ^{13}C , (c) ^{15}N , (d) ^{17}O , and (e) ^{19}F , respectively.

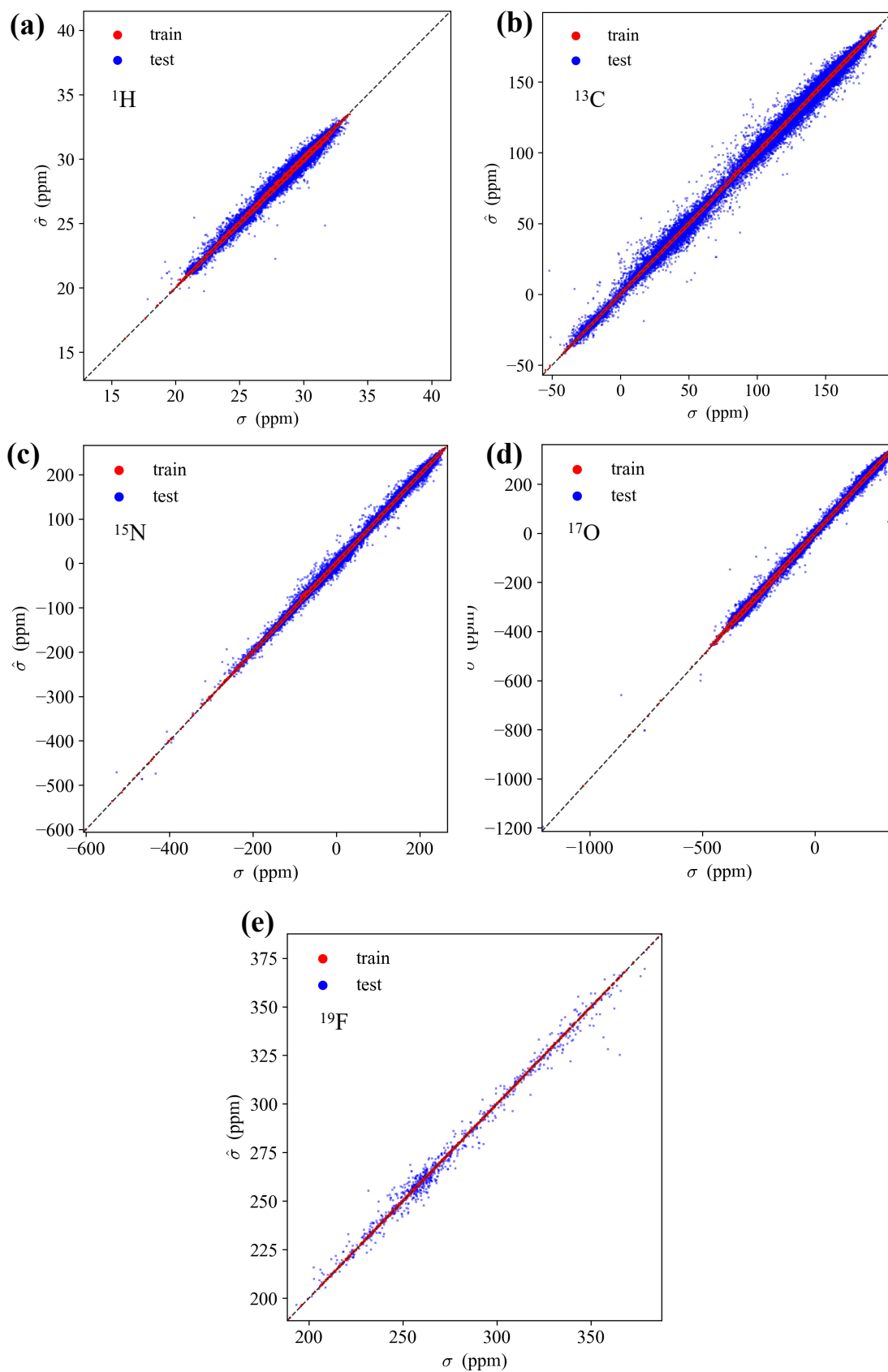


FIG. 5. Scatterplots for the training set (red) and test set (blue) showing NMR chemical shifts from the QM9NMR dataset, using the M3GNet GNN-TF/KRR model constructed with QM9NMR data for the five elemental species: (a) ^1H , (b) ^{13}C , (c) ^{15}N , (d) ^{17}O , and (e) ^{19}F , respectively.

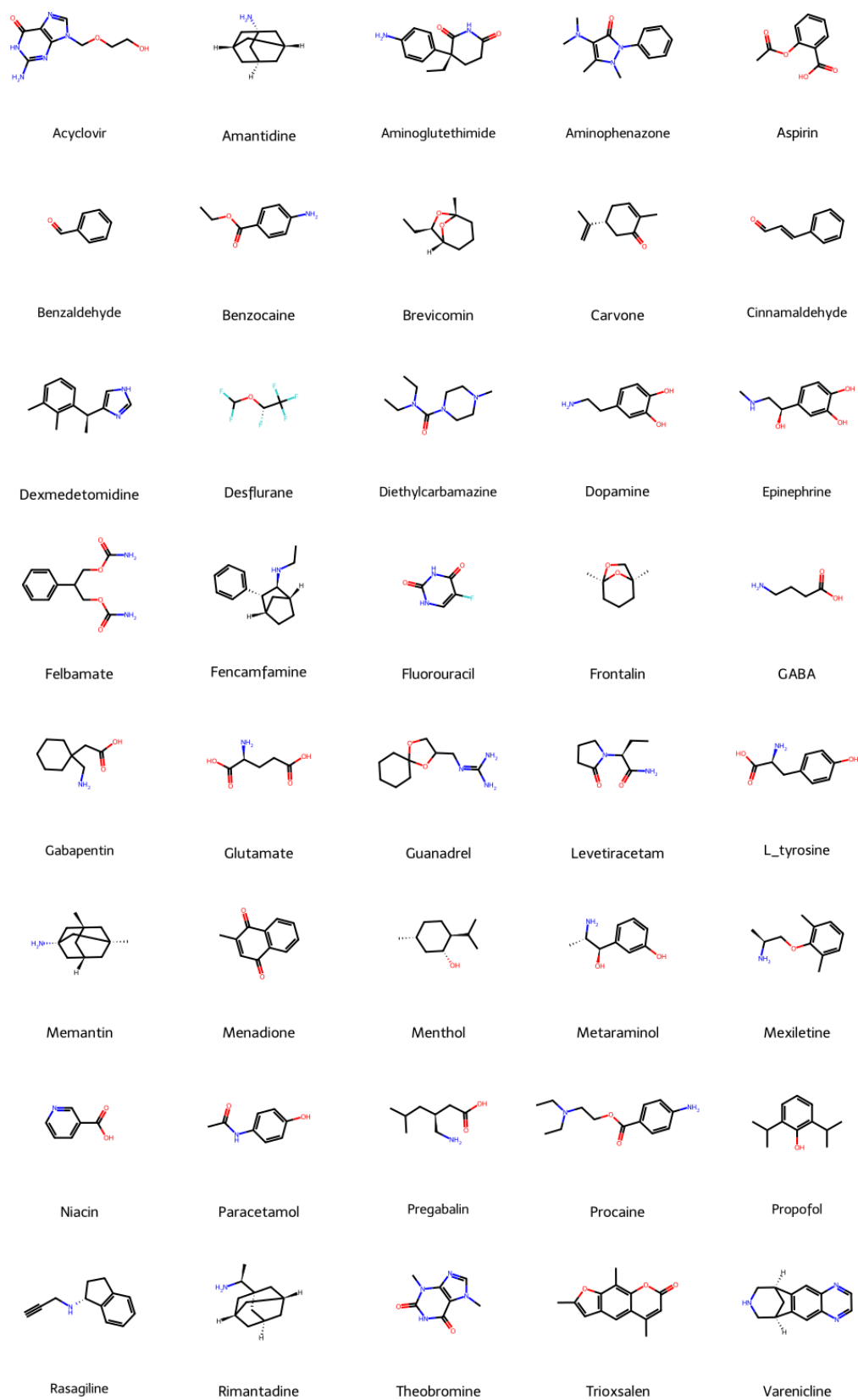


FIG. 6. Structures of the test set, consisting of 40 drug molecules from the GDB17 universe.

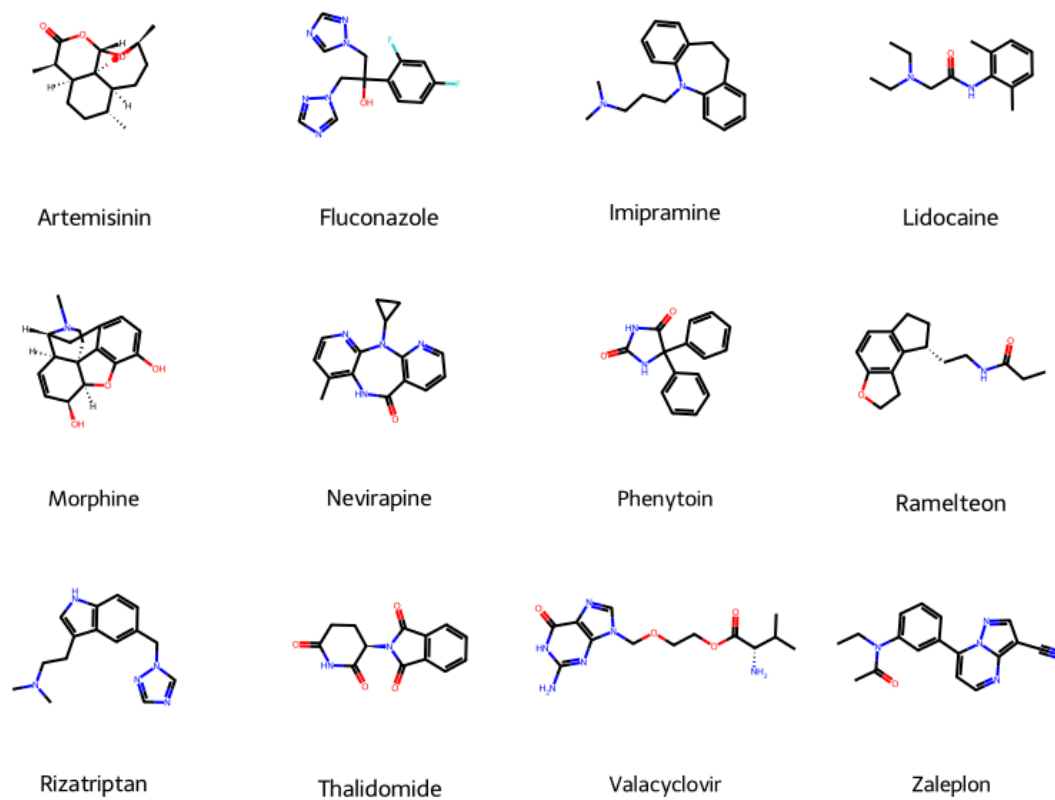


FIG. 7. Structures of the test set, consisting of 12 drugs with 17 or more heavy atoms.

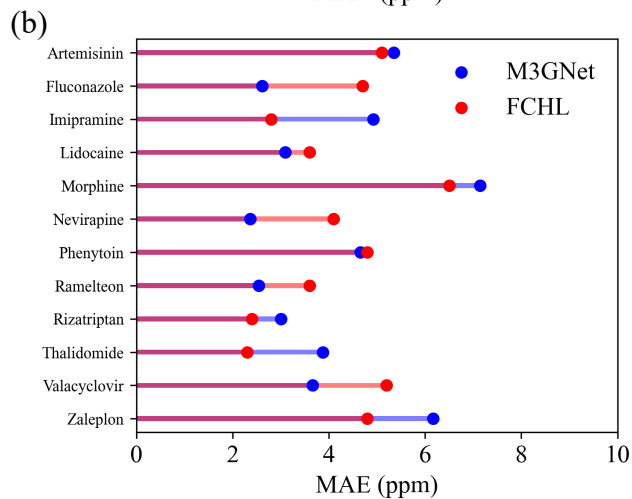
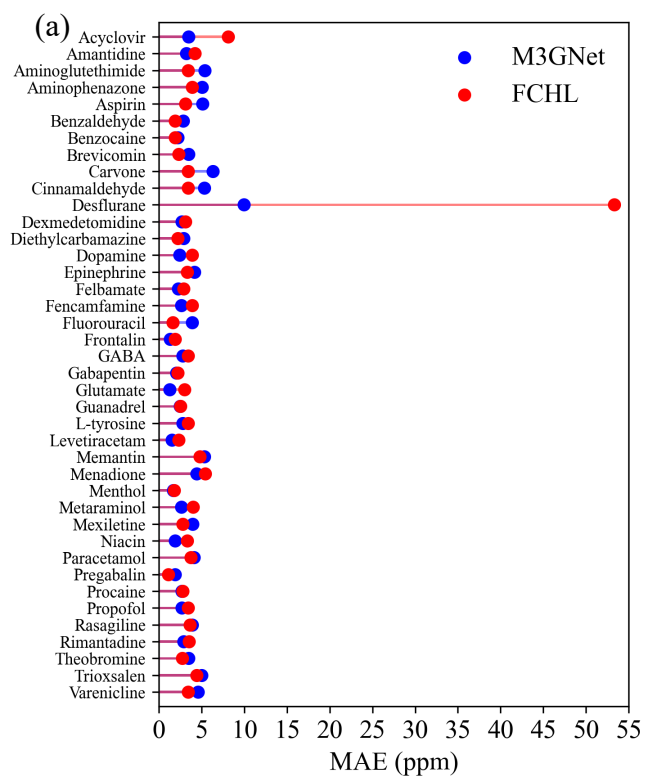


FIG. 8. Comparison of ^{13}C NMR shielding constant predictions using different descriptors for (a) 40 drug molecules from the GDB17 universe and (b) 12 drugs with 17 or more heavy atoms. The predictions were made using the KRR model with the FCHL descriptor (red) and the M3GNet GNN-TF descriptor (blue), respectively. FCHL results were taken from a separate study.[29]